Mechanistic Investigations into the Enantioselective Conia-Ene Reaction Catalyzed by Cinchona-Derived Amino Urea Pre-Catalysts and Cu(I.)

ARTICLE *in* CHEMISTRY - A EUROPEAN JOURNAL · SEPTEMBER 2013

Impact Factor: 5.73 · DOI: 10.1002/chem.201200832 · Source: PubMed

7 AUTHORS, INCLUDING:

Filippo Sladojevich

25 PUBLICATIONS **461** CITATIONS

SEE PROFILE

Angel Fuentes

Universidad de Salamanca

22 PUBLICATIONS **151** CITATIONS

SEE PROFILE

Robert S Paton

University of Oxford

68 PUBLICATIONS **1,051** CITATIONS

SEE PROFILE

DOI: 10.1002/chem.201200832

Mechanistic Investigations into the Enantioselective Conia-Ene Reaction Catalyzed by Cinchona-Derived Amino Urea Pre-Catalysts and Cu^{I}

Filippo Sladojevich,[a] Ángel L. Fuentes de Arriba,[b] Irene Ortín,[a] Ting Yang,[c] Alessandro Ferrali,[d] Robert S. Paton,*[a] and Darren J. Dixon*[a]

Abstract: The enantioselective Conia-ene cyclization of alkyne-tethered β-ketoesters is efficiently catalyzed by the combination of cinchona-derived amino-urea pre-catalysts and copper(I) salts. The reaction scope is broad and a series of substrates can be efficiently cyclized with high yields and enantioselectivities. Herein, we present a detailed mechanistic study based on experimental considerations and quantum mechanical calculations. Several variables, such as the nature of the organic pre-catalyst and the metal-ion source, have been thoroughly investigated. Kinetic studies, as well as kinetic isotope effects and deuterium labeling experiments have been used to gain further insights into the mechanism and prove the cooperative nature of the catalytic system. Our studies suggest that the rate-limiting step for the reaction involves the β-ketoester deprotonation and that the active species responsible for the enantiodetermining step is monomeric in amino-urea pre-catalyst. Computational studies provide a quantitative understanding of the observed stereoinduction and identify hydrogen bonding from the urea group as a crucial factor in determining the observed enantioselectivity.

Keywords: asymmetric catalysis · cinchona alkaloids · Conia-ene reaction · quantum mechanical calculations · reaction mechanism

Introduction

Cooperative catalysis is a powerful tool in asymmetric synthesis, allowing access to new chemical reactivity and providing high stereocontrol in a wide range of reactions. Through mutual activation and organization of reagents, this concept has been applied widely to reactions of nucleophilic and electrophilic species, by the combination of (Lewis/Brønsted) acids and bases distributed around a chiral scaffold.[1] A thriving research area in the field of cooperative catalysis has emerged, in which organocatalysts and transition-metal ions are combined.[2] This combination presents the opportunity to explore new reaction pathways by combining organocatalytic activation (such as enamine activation or acid/base activation) with transition-metal-ion-catalyzed processes. We reasoned that cinchona-derived structures, such as **1a**–**d**[1d,3] could perform, in combination with different transition-metal ions, as cooperative catalytic systems (Figure 1).

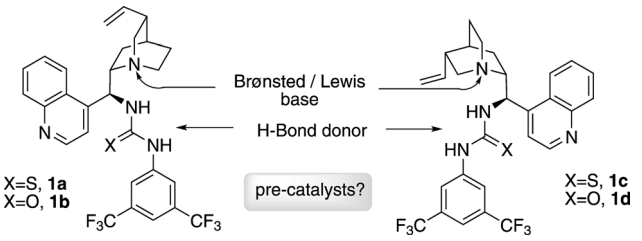

Figure 1. Pseudoenantiomeric cinchona-derived potential pre-catalysts **1a**–**d**.

Since bifunctional catalysts **1a**–**d** are effective in promoting nucleophilic addition of active methylene compounds,[1d] we hypothesized that **1a**–**d** could be effective in generating enolates of β-ketoesters and we postulated that such enolates, in the presence of appropriate metal ions, would exhibit reactivity towards an alkyne functionality. We recently examined the asymmetric Conia-ene reaction of β-ketoesters as a platform for this cooperative catalysis concept.[4] We demonstrated that the combination of **1b** and $CuOTf\cdot{}^{1}/_{2}C_6H_6$ is an effective catalytic system for the enantioselective cyclization of alkyne-linked β-ketoesters and β-ketoamides.[5] Notably, this new catalytic system represents

[a] Dr. F. Sladojevich, Dr. I. Ortín, Dr. R. S. Paton, Prof. D. J. Dixon
Chemistry Research Laboratory, Department of Chemistry
University of Oxford
Mansfield Road, Oxford, OX1 3TA (U.K.)
E-mail: robert.paton@chem.ox.ac.uk
darren.dixon@chem.ox.ac.uk

[b] Á. L. Fuentes de Arriba
Organic Chemistry Department
University of Salamanca
Plaza de los Caídos 1-5, Salamanca, 37008 (Spain.)

[c] Dr. T. Yang
GlaxoSmithKline (China) R&D
Building No. 3, 898 Halei Road Zhangjiang Hi-tech Park,
Pudong Shanghai 201203 (China.)

[d] Dr. A. Ferrali
Enantia S.L.
C/Baldiri Reixac, 1008028 Barcelona (Spain.)

Supporting information for this article is available on the WWW under http://dx.doi.org/10.1002/chem.201200832.

one of the few examples able to promote the carbocyclization at room temperature. Intrigued by this new reactivity, we decided to start further studies to prove the cooperativity of the catalytic system and gain a better picture of the activation mode. We believed that the knowledge gained could be insightful for future research projects in the field of asymmetric cooperative catalysis.

Herein, we report a detailed mechanistic study based on various experimental and computational data. In particular, we elucidate the effect of the pre-catalyst's structure on the reaction rate and enantioselectivity and elucidate the effects of the urea hydrogen-bonding capability on acceleration of the reaction rate. A kinetic study, kinetic isotope effects, nonlinear and titration studies are used to gain insight into the mechanism and demonstrate the cooperativity of the new catalytic system and to identify the rate-determining step. Finally, computational studies contribute to elucidate the mechanistic steps and origin of enantioselectivity from a qualitative and quantitative point of view.

Results and Discussion

Initially, the influence of various metal sources, pre-catalysts and solvents on the reaction outcome was investigated and the reaction scope surveyed by using the optimal conditions identified.

Metal screening: A metal screen was carried out on the easily synthesized substrate **2a** (Table 1). Different transition-metal salts were screened in conjunction with pre-catalyst **1b** in dichloromethane. Conversions were measured after 18 h by ^{1}H NMR spectroscopy. To our surprise, [AuCl(PPh$_3$)]/AgOTf and AgOTf gave no product after 18 h (Table 1, entries 1 and 2). Zn(OTf)$_2$ gave 31% conversion with a low enantioselectivity (6% *ee* (*ee* = enantiomeric excess; Table 1, entry 3). [NiCl$_2$(dppe)] (dppe = 1,2-bis(diphenylphosphino)ethane) furnished the enantiomeric product in 68% conversion and in 30% *ee* (entry 4). Pleasingly, CuOTf·$^1/_2$C$_6$H$_6$ gave 92% *ee* with 82% conversion (entry 5). Once copper(I) was identified as the metal ion of choice, a wide range of copper sources was tested in the reaction. Similar reactivity was observed with different copper(I) salts (entries 5–8).

Table 1. Screening of metal sources.

Entry	[ML$_n$]	t [h]	Conv. [%]	*ee* [%]
1	[AuCl(PPh$_3$)]/AgOTf	18	0	–
2	AgOTf	18	0	–
3	Zn(OTf)$_2$	18	31	+6
4	[NiCl$_2$(dppe)]	18	68	−30
5	CuOTf·$^1/_2$C$_6$H$_6$	18	82	+92
6	CuCl	18	99	+92
7	CuBr	18	98	+92
8	CuI	18	94	+92
9	CuCN	18	11	+91

Interestingly, the enantioselectivity was not influenced by the nature of the counteranion, which suggested that in all cases the same, highly organized stereodetermining transition structure is formed, independent of the counteranion. When CuCN was used, the reaction rate decreased considerably but the enantiomeric excess of the product was 91%, which suggested that the rate-determining step differs from the enantiodetermining step (the carbocyclization). It is important to note that the cyclization of **2a** in the presence of CuOTf·$^1/_2$C$_6$H$_6$ yields the desired product **3a** with the same enantioselectivity and yield as CuCl, CuBr or CuI and each salt can be used indifferently. CuOTf·$^1/_2$C$_6$H$_6$ was selected as the copper source in subsequent studies (even though it displayed a slightly diminished reaction rate relative to CuCl and CuBr) to allow direct comparisons with earlier results obtained using the same copper source.

Pre-catalyst screen: A substantial screen of pre-catalysts was carried out (Table 2) to gain further mechanistic insights and identify structure–activity relationships.

Different hydrogen-bond donors were compared. Ureas **1b** and **1d–l** were found to be the most effective pre-catalysts but amides **1m–q** were also moderately effective in promoting the carbocyclization of substrate **2a** to afford **3a** with appreciable levels of enantioselectivity, although with decreased reaction rate. Sulphonamide **1r** was found to be a poor pre-catalyst, giving rise to only traces of product after 24 h. Also thiourea **1a** and pseudoenantiomeric **1c** were not active, presumably due to strong ligation of the copper catalyst by the sulphur atom of the thiourea group. Different substituents on the urea aromatic ring were also investigated. When the series of *para*-substituted ureas **1g–l** was considered, it was clear that electron-withdrawing groups have a remarkable effect in accelerating the reaction: *p*-OMe-substituted urea **1i** gave 26% conversion after 1 day, whereas urea **1l**, bearing a *p*-nitro group, gave rise to 87% conversion in the same amount of time. These results strongly suggest that the acidity of the urea N−H bonds is correlated with reactivity. Finally, the relative stereochemistry at C-8 and C-9 was investigated. For this purpose urea **1s**, with inverted stereochemistry at C-9 (with respect to **1b**), was prepared.[6] Notably, pre-catalyst **1s** gave rise to lower conversion and enantioselectivity, proving that the relative orientation of the bridgehead nitrogen atom and the urea is essential for the high levels of enantioselectivity and reactivity observed, consistent with a cooperative mode of action.

Solvent effect: The influence of solvents on the reaction outcome was also studied. Dichloromethane was confirmed as the ideal solvent from a point of view of reactivity and enantioselectivity. Nevertheless, the reaction was tolerant to the nature of the solvent, showing identical conversion and a small erosion in enantioselectivity when performed in toluene. A polar protic solvent, such as MeOH, could also be used without any loss in enantioselectivity, albeit at a lower reaction rate (Table 3).

Table 2. Screening of pre-catalysts.

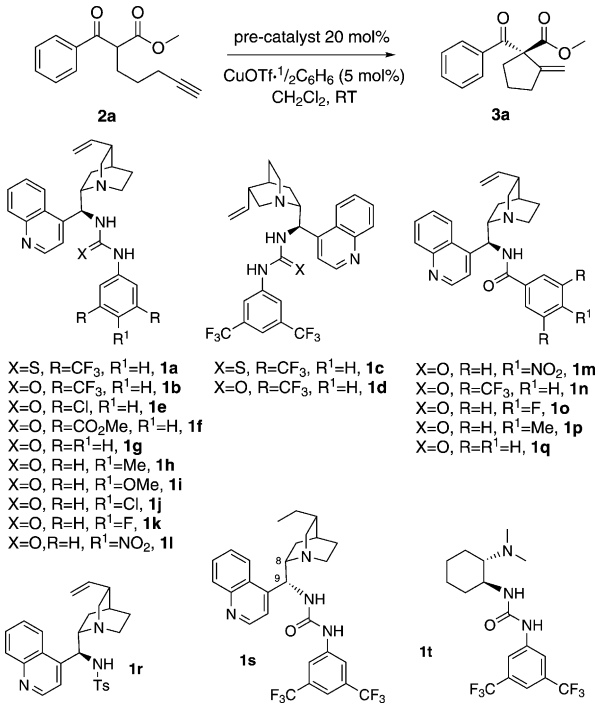

Entry	Pre-catalyst	*t* [h]	Conv. [%]	*ee* [%]
1	**1a**	24	0	–
2	**1b**	24	98	92
3	**1c**	24	0	–
4	**1d**	24	92	−89
5	**1e**	24	86	93
6	**1f**	24	80	83
7	**1g**	24	39	81
8	**1h**	24	31	84
9	**1i**	24	26	80
10	**1j**	24	58	85
11	**1k**	24	50	82
12	**1l**	24	87	94
13	**1m**	24	2	61
14	**1n**	24	3	68
15	**1o**	24	2	–
16	**1p**	24	3	37
17	**1q**	24	2	53
18	**1r**	24	traces	–
19	**1s**	24	46	−5
20	**1t**	24	25	81

Table 3. Solvent effects.

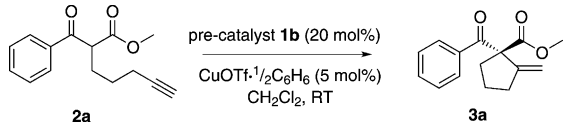

Entry	Solvent	*t* [h]	Conv. [%]	*ee* [%]
1	CH_2Cl_2	24	98	92
2	toluene	24	98	88
3	MeOH	24	51	93
4	DMSO	24	0	–

Highly coordinating DMSO was found to be incompatible with the catalytic system and no product was observed when it was used as the solvent, presumably due to quenching of the metal ion Lewis acidity resulting from complexation of the highly coordinating DMSO.[7] Alternatively, DMSO might interfere with the urea hydrogen-bonding capability.[8]

Substrate scope: With optimal reactivity and enantiocontrol established, the scope of the reaction was surveyed by using 20 mol% of either pre-catalyst **1b** or pseudoenantiomeric **1d** and 5 mol% of CuOTf·$^1/_2C_6H_6$ in dichloromethane at room temperature. A range of pentynyl β-ketoesters incorporating significant structural and electronic diversity to both the ester and ketone group was investigated and the results are presented in Table 4.

The reaction was general for aliphatic and (electron-rich or -poor) aromatic β-ketoester substrates. The steric demand of the ester group had little effect on the reaction enantioselectivity (Table 4, entries 1–3). Similarly, aryl amides were also good substrates in the process (entry 18). Reaction times reflected in part the acidity of the substrates with the fastest finishing after one day and slowest after 10 days. Enantiomeric excesses ranged from 79–93% with the highest arising from aryl ketone substrates. The substitution of **1b** for pseudoenantiomeric pre-catalyst **1d** in the cyclization reaction of **2a** afforded (*S*)-**3a** in good yield and enantiocontrol (entry 19, 92% yield, 89% *ee*); **2o** yielded (*S*)-**3o** in an improved yield but with a slightly diminished *ee* of 74% (entry 20 vs. 15). Single-crystal X-ray analysis on **3k** and a spirocyclic derivative of **3o**, as well as chemical correlation studies on **3p** established the *R* configuration of these compounds when pre-catalyst **1b** was employed;[4a] the rest were assigned by analogy. Aromatic β-ketoesters presenting substitution of the terminal alkyne position (with aromatic or aliphatic substituents) were found to be unreactive under the reported reaction conditions. A similar outcome was observed when β-ketoesters giving rise to six- or seven-membered rings were used. β-Diketones giving rise to five-membered rings were found to be suitable substrates and were cyclized under the reported reaction conditions but in moderate enantiomeric excess. For example 2-(pentynyl)-1-phenylbutane-1,3-dione was cyclized completely (98% conversion after two days) under optimal reaction conditions in 45% *ee*.

Stereochemical outcome of deuterated substrates: Further mechanistic insight was gained by repeating the reaction with monodeuterated substrate **4**.

At low conversion,[9] the predominant monodeuterated product was (*E*)-**7**. This is consistent with the intermediacy of a ligated copper enolate that undergoes an enantioselective *syn*-carbocupration followed by a final protodemetallation step as shown in Scheme 1.[5b]

Kinetic measurements: Kinetic profiles were determined at different copper and pre-catalyst loadings. Conversion was measured by ^{1}H NMR spectroscopy after 16 h in CD_2Cl_2. First, the amount of CuOTf·$^1/_2C_6H_6$ was fixed at 5 mol% and a series of reactions were performed whilst the loading

Table 4. Scope of the catalytic asymmetric Conia-ene reaction.

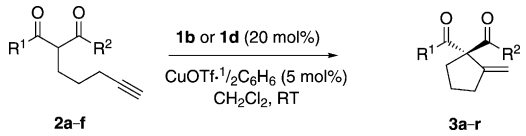

Entry	Product	R^1	R^2	Pre-cat.	*t* [days]	Yield [%]	*ee* [%]
1	(*R*)-**3a**	Ph	OMe	**1b**	1.5	98	92
2	(*R*)-**3b**	Ph	OEt	**1b**	1.5	82	91
3	(*R*)-**3c**	Ph	OBn	**1b**	1.5	95	89
4	(*R*)-**3d**	4-Me-C_6H_4	OMe	**1b**	3	97	92
5	(*R*)-**3e**	3-Me-C_6H_4	OMe	**1b**	2	99	92
6	(*R*)-**3f**	2-Me-C_6H_4	OMe	**1b**	1	67	87
7	(*R*)-**3g**	4-MeO-C_6H_4	OMe	**1b**	10	91	91
8	(*R*)-**3h**	3-MeO-C_6H_4	OMe	**1b**	1.5	96	93
9	(*R*)-**3i**	4-F-C_6H_4	OMe	**1b**	4	74	92
10	(*R*)-**3j**	2-F-C_6H_4	OMe	**1b**	1	77	89
11	(*R*)-**3k**	4-Br-C_6H_4	OMe	**1b**	1	87	93
12	(*R*)-**3l**	3,4-di-Cl-C_6H_3	OMe	**1b**	1	83	92
13	(*R*)-**3m**	4-Ph-C_6H_4	OMe	**1b**	1	89	89
14	(*R*)-**3n**	2-naphthyl	OMe	**1b**	2	84	91
15	(*R*)-**3o**	Me	OEt	**1b**	1.5	85	83
16	(*R*)-**3p**	Me	OBn	**1b**	1.5	67	80
17	(*R*)-**3q**	Et	OMe	**1b**	3.5	77	79
18	(*R*)-**3r**	Ph	NHPh	**1b**	5	85	83
19	(*S*)-**3a**	OMe	Ph	**1d**	2	92	−89
20	(*S*)-**3o**	OEt	Me	**1d**	2	90	−74

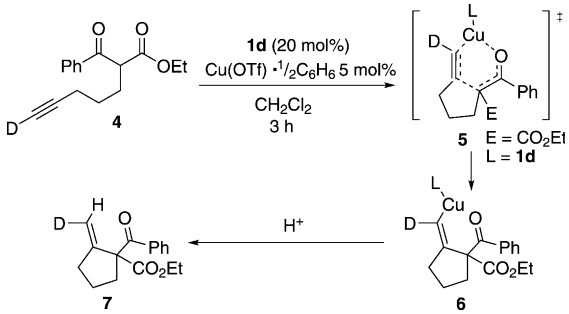

Scheme 1. Reaction outcome with deuterated substrate **4**.

of the pre-catalyst **1b** was varied (Figure 2). Next the amount of pre-catalyst **1b** was fixed at 20 mol% and the CuOTf·$^1/_2C_6H_6$ was varied in the range of 0–40 mol%.

Interestingly, on increasing the copper loading (above 5 mol%), the reaction rate decreased. We hypothesize that at high copper loading the basic sites of the pre-catalyst are preferentially ligated to the metal ion and, therefore, pre-catalyst **1b** is not able to act as a Brønsted base in the deprotonation of the β-ketoester. Increasing the loading of pre-catalyst **1b** at a fixed 5 mol% of CuOTf·$^1/_2C_6H_6$ gave rise to a linear increase in the reaction rate in the range of 5–30 mol% (grey diamonds in Figure 2). Next, the order of reaction with respect to each of the components was studied. The reaction was found to be first order in the substrate as illustrated in Figure 3. With *ln*[**2a**] plotted against time, a linear relation is clearly shown, typical of a first-order kinetic profile with respect to the substrate. The order of reaction with respect to CuOTf·$^1/_2C_6H_6$ and pre-catalyst **1b** was then investigated using the initial rates method (Figure 4). The rate dependence on the concentration of copper ions was studied at a fixed concentration of pre-catalyst **1b** of 0.02 M (20 mol% with respect to β-ketoester **2a**) by varying the percentage of CuOTf·$^1/_2C_6H_6$ in the region of 0.64–4.00 mol%. Inhibition due to copper ions was less pronounced in this concentration range, as shown in Figure 2. The reaction order with respect to CuOTf·$^1/_2C_6H_6$ was found to be 0.36, confirming that a series of equilibria is involved in the reaction mechanism. The reaction order with respect to pre-catalyst **1b** was studied at a fixed concentration of CuOTf·$^1/_2C_6H_6$ (0.005 M) in a 5 mol% ratio with respect to β-ketoester **2a**. The reaction

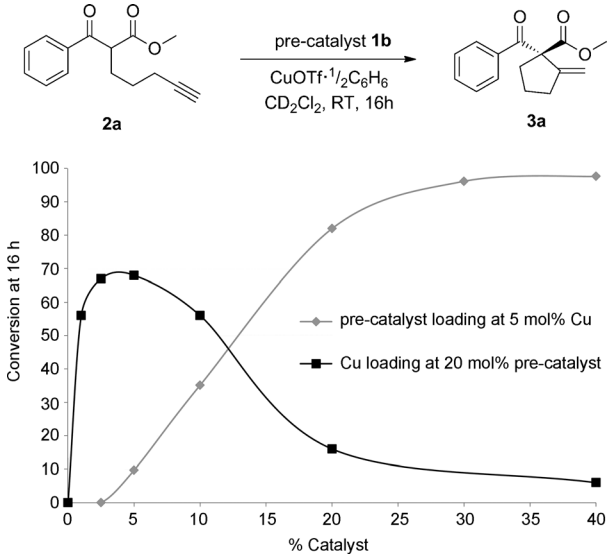

Figure 2. Conversion as a function of loading of CuOTf·$^1/_2C_6H_6$ and pre-catalyst **1b**.

order with respect to pre-catalyst **1b** was found to be 1 in the range of concentration 0.00967–0.0392 M (10 to 40 mol% with respect to β-ketoester **2a**). To establish the rate-determining step in the reaction, kinetic isotope measurements were considered. Mono- and bis-deuterated substrates **8** and **9** (Figure 5) were tested under the standard reaction conditions (0.1 M, 20 mol% of pre-catalyst **1b** and 5 mol% of CuOTf·$^1/_2C_6H_6$). Here it should be pointed out that deuterium scrambling is observed between the C_α–H of the ketoester and the alkyne C–D, so the use of a doubly deuterat-

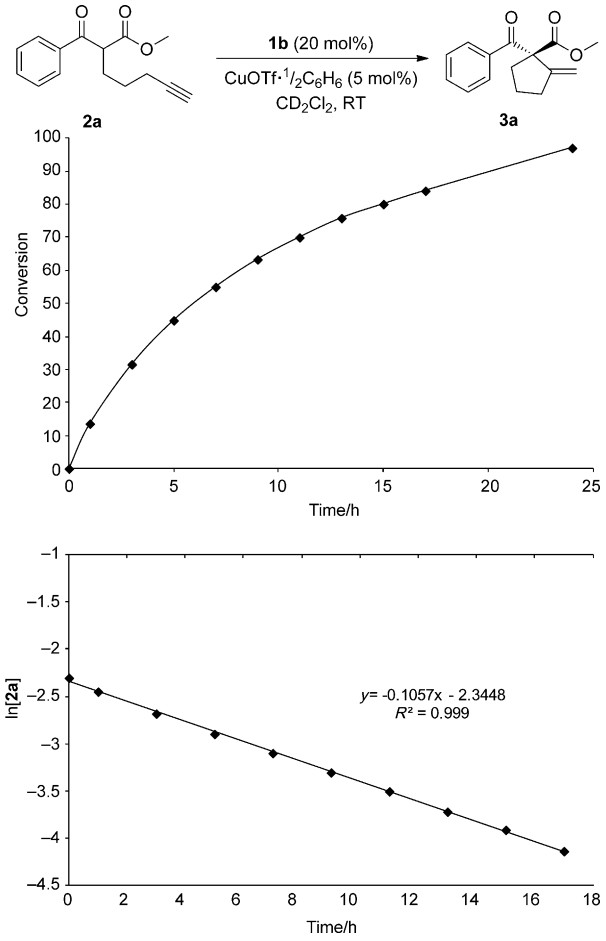

Figure 3. Substrate reaction order.

ed substrate was envisaged to establish whether or not the carbon–carbon bond-forming step was rate-determining.

When mono-deuterated substrate **8** was used, a primary kinetic isotope effect was observed in the initial rate (k_H/k_D=3.9). When doubly deuterated substrate **9** was used, a primary kinetic isotopic effect was also observed (k_H/k_D= 4.5), which suggested that the rate-determining step is not the carbocyclization step. This is further supported by the fact that no correlation between enantioselectivity and reaction rate is observed. For example, for all the points of the graphic in Figure 2, the product is always formed with a constant enantiomeric excess of 92%. The observed kinetic isotope effect suggests that the rate-determining step involves the breaking of a bond to hydrogen. In this case, two possible scenarios emerge: 1) the rate-determining step is the deprotonation of the C_α–H bond of β-ketoester **2a** or 2) the rate-determining step is a protonation event occurring after the C–C bond formation; in this case the kinetic isotope effect would be related to the breaking of a N–D bond of the protonated bridgehead ammonium enolate formed after the initial deprotonation of the β-ketoester. To discern between these two possibilities, we measured the carbon isotope effect employing Singleton's NMR spectroscopic technique at natural abundance.[10] ^{13}C NMR spectra were meas-

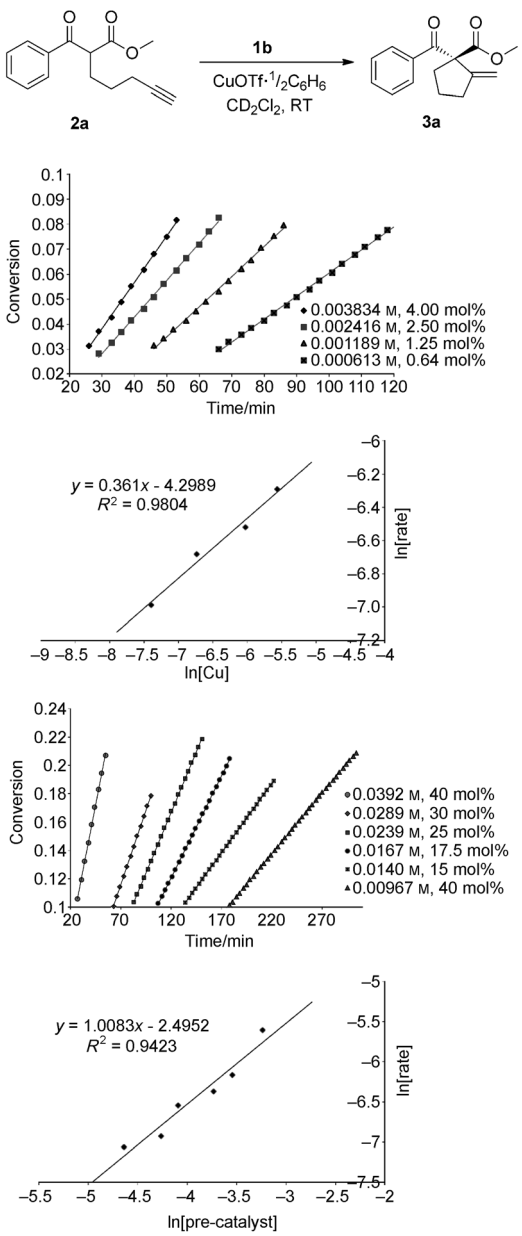

Figure 4. Reaction order for CuOTf·$^1/_2$ C_6H_6 and pre-catalyst **1b**.

ured for the virgin starting material **2a** and then for the recovered **2a** after the reaction was run for 48 h (97% conversion). An enrichment in ^{13}C for a given carbon atom of the recovered starting material indicates that the carbon atom is involved in a bond that is broken in the rate-limiting step. The ratio of integrals between recovered **2a** and virgin **2a** (as the average of three runs) is reported in Scheme 2. A pronounced kinetic isotope effect (1.043) was observed for the C_α atom of recovered β-ketoester **2a** in comparison to all other carbon atoms (Scheme 2).

To gain further insight into the deprotonation event, the rate of substrate racemization was also monitored. Initially, (+)- and (−)-**2a** were treated separately with pre-catalyst **1b** (in the absence of a copper salt) and the specific rotation, $[\alpha]_D$, was measured as a function of time. As shown in

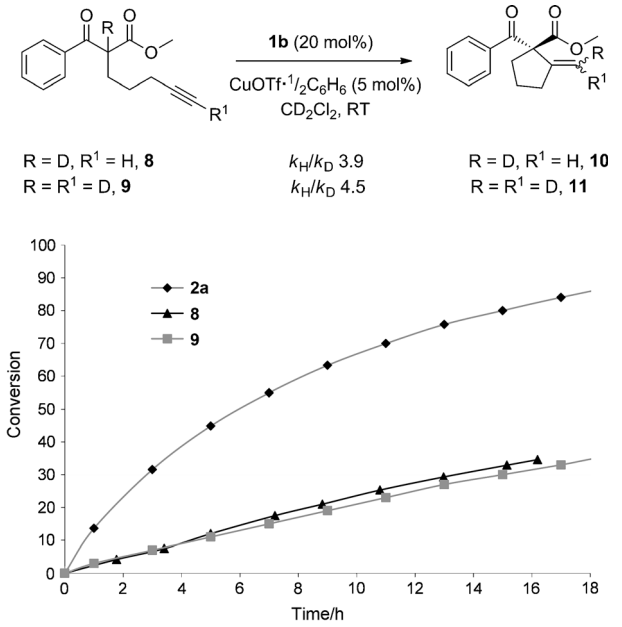

Figure 5. Kinetic isotopic effect for substrates **8** and **9**.

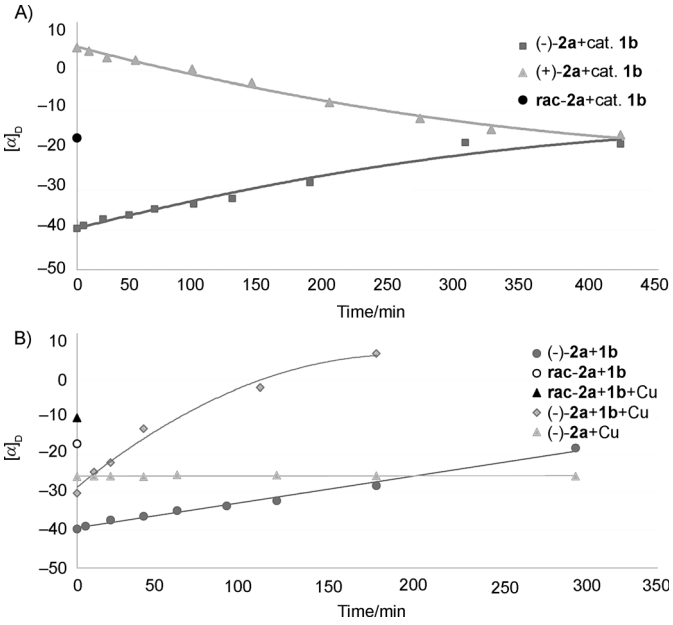

Figure 6. A) Racemization rate of (+)- and (−)-**2a** in the presence of pre-catalyst **1b**. B) Racemization rate of (−)-**2a** in the presence of pre-catalyst **1b** and in the presence of pre-catalyst **1b** and CuOTf·$^1/_2$C$_6$H$_6$.

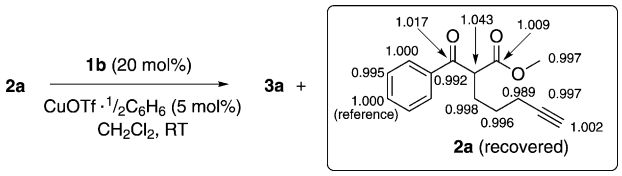

Scheme 2. Natural abundance ^{13}C kinetic isotope effect measured at 97% conversion.

Figure 6A, the rates of racemization of enantiomeric β-ketoesters, (+)- and (−)-**2a** in the presence of **1b** were essentially the same: both substrates were fully racemized within 7 h, forming the same product mixture with **1b**. This demonstrates that enolization by the pre-catalyst in the absence of Cu is rapid on the timescale of the reaction (typically 24–48 h). Figure 6B shows the change in specific rotation in the presence of Cu^I, with and without the addition of pre-catalyst **1b**. Racemization was not observed unless both Cu^I and pre-catalyst were present.

The measured primary D/H and ^{13}C/^{12}C KIEs both indicate that the RDS involves breaking the α-C–H bond. In the presence of Cu^I, this suggests that formation of the Cu-enolate is rate-limiting. Enolization of substrate by pre-catalyst **1b** is competitive and does not require Cu^I; however, this is unproductive and does not lead to cyclization.

Pre-catalyst role: To further understand the role of pre-catalyst **1b** in the reaction mixture, we decided to replace **1b** with a combination of an organic base (either quinuclidine or 2-*tert*-butylimino-2-diethylamino-1,3-dimethylperhydro-1,3,2-diazaphosphorine (BEMP)) and model urea **12** or **13** (Figure 7A). This idealized system was designed to gain further insight into the role of the tertiary amine and the urea moieties and has been used to understand if the urea is playing an active role or if the active catalytic site on pre-catalyst **1b** is only the tertiary amine. Figure 7A shows the reaction conversion at a fixed amount of 5 mol% of CuOTf·$^1/_2$C$_6$H$_6$ and 20 mol% of organic base (either quinuclidine or BEMP), when the loading of ureas **12** or **13** is varied in the range of 0–50 mol%. This clearly illustrates that cyclic urea **13** is completely inactive in catalyzing the reaction, whereas urea **12**, with two N–H protons capable of forming hydrogen-bonding interactions, increases the reaction rate upon an increase in loading. A second point that emerges is that conversion in the presence of BEMP is much higher than in the presence of quinuclidine. This data is in good agreement with the difference in pK_{BH+} between the two bases[11] and in support of a rate-determining enolization step. We then looked at the conversion when urea **12** and CuOTf·$^1/_2$C$_6$H$_6$ were fixed at 20 and 5 mol%, respectively, and the amount of BEMP was varied in the range of 0–50 mol% (Figure 7B).

In the absence of base (0 mol% of BEMP) no reaction is observed and this data is in agreement with the cooperative nature of the catalytic system, in which both a urea and an organic base are required for the reaction to occur. Interestingly, when the base loading is higher than the loading of urea **12**, a decrease in the reaction rate is observed. One possible hypothesis is that deleterious complexation of Cu^I with excess BEMP lowers the amount of reactive copper in the reaction mixture.[12]

The graphics in Figure 7 demonstrate that the observed rate acceleration due to amino-urea **1b** is not simply a

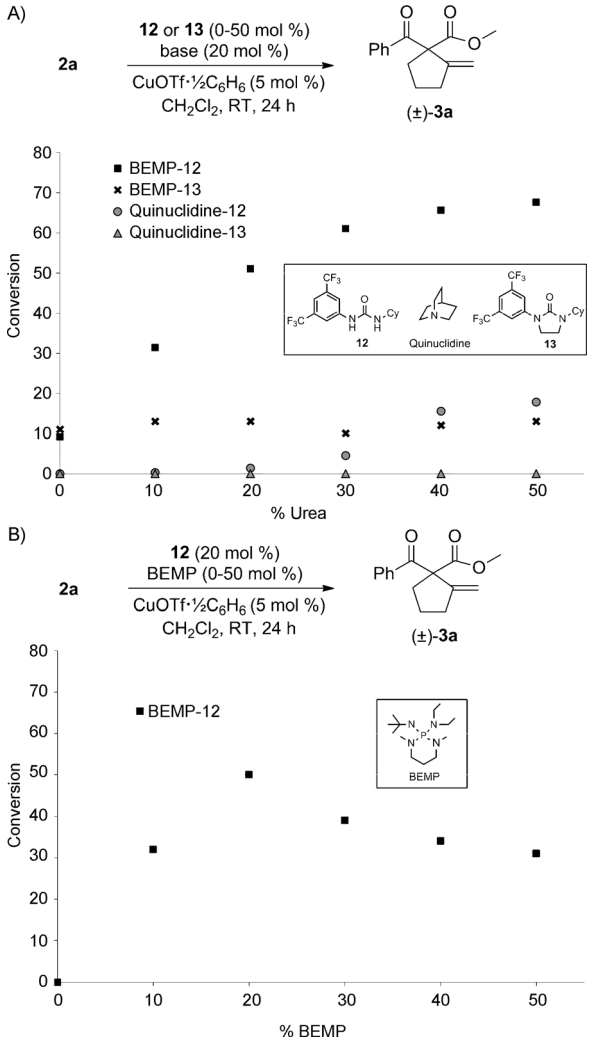

Figure 7. A) Conversion studies at different loadings of ureas **12** and **13** in the presence of BEMP or quinuclidine. B) Conversion studies at different loadings of BEMP in the presence of 20 mol% of urea **12**.

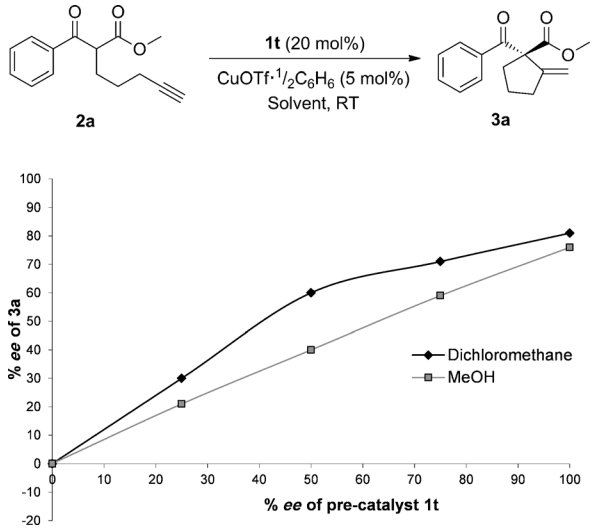

Figure 8. Nonlinear effect between *ee* of pre-catalyst **1t** and *ee* of product **3a** in CH_2Cl_2 and MeOH.

ligand effect on the Cu: when pre-catalyst **1b** is 'split' into two separate chemical entities the presence of both urea and basic functional groups are essential in maintaining catalytic activity, which suggests that pre-catalyst **1b** is promoting enolization by acting as a Brønsted base and as a hydrogen-bond donor.

Origins of enantioselectivity: Further experiments were required to gain a better understanding of the enantio-determining step and an investigation of possible nonlinear effects[13] was performed. The enantiomer of pre-catalyst **1b** was not readily available. Therefore, we performed these experiments with pre-catalyst **1t**,[14] easily available in both enantiomeric forms. The *ee* value of product **3a** was studied as a function of the *ee* value of pre-catalyst **1t** (Figure 8). A linear correlation would imply that the chiral species responsible for asymmetric induction is monomeric in the enantio-determining step. In contrast, a nonlinear relationship implies that the active chiral catalyst is formed by association of the pre-catalyst into diastereomeric aggregated species in solution. Given the formation of precipitates in the reaction mixture (especially when CH_2Cl_2 is used as the solvent), two sets of experiments were performed, using either CH_2Cl_2 or MeOH.

Figure 8 shows that a linear correlation is observed when MeOH is used as the solvent, whereas a slight positive nonlinear relationship between the two enantiomeric values is obtained using CH_2Cl_2. This suggests that the active catalytic species responsible for asymmetric induction is monomeric; however, the nonlinear effect observed in CH_2Cl_2 is most likely due to solubility effects,[15] which are particularly accentuated in the chlorinated solvent (when catalyst **1t** was mixed with an equimolar amount of its enantiomer in CH_2Cl_2 the formation of a crystalline precipitate is clearly observed).

Modeling studies: To aid in the interpretation of our experimental studies and to shed light on the origins of enantioselectivity, we performed quantum chemical calculations by using DFT with Gaussian 09.[16] The M06-2X meta-hybrid GGA density functional[17] was used for geometry optimization and, along with B3LYP,[18] for single-point energy calculations. The M06-2X functional was chosen in this study as it has been parameterized to treat dispersion interactions, that are entirely absent from the (older) hybrid GGA functionals.[19] Such non-covalent interactions are expected to be important for asymmetric induction,[20] barrier heights and reaction energies over an uncorrected hybrid GGA functional, such as B3LYP.

Restricted Kohn–Sham DFT calculations were used throughout.[21] For all geometry optimizations the Pople all-electron 6-31G(d) double-ζ valence basis set was employed for C, H, N, O and F atoms in combination with the Hay Wadt LANL2DZ effective core potential[22] (ECP) and double-ζ valence basis for Cu. A larger 6-311+G(d,p)

triple-ζ valence basis set and LANL2TZ(f) ECP plus triple-ζ valence basis combination was used for single-point energy calculations.[23] An ultrafine (99,590) grid containing 99 radial shells and 590 angular points per shell was used for the numerical integration in the calculation of single-point energetics.[24] Stationary points were verified as minima (zero imaginary frequencies) or transition structures (a single imaginary frequency) with harmonic frequency calculations at the same level of theory as optimizations, and Gibbs free energies were computed at 298 K after shifting very low frequencies below 50 cm^{-1} to a value of 50 cm^{-1} to prevent spuriously large vibrational entropic terms. Due to the insensitivity of conversion and enantioselectivity with respect to the solvent observed in our experiments, optimizations were performed in the gas phase; however, the effects of solvation have been included through single-point energy calculations with a CPCM model by using UAKS radii.[25] Where applicable, all possible efforts were made to find the lowest-energy conformations by performing geometry optimizations from different starting points. Natural bond orbital (NBO) calculations were performed with NBO 3.1[26] and Wiberg bond orders computed.[27]

To gain a qualitative and quantitative understanding of the observed stereoinduction we modeled competing stereodetermining C–C bond-forming transition structures (TSs) by using quantum chemical calculations. The nature and geometry of this TS were established by performing calculations on a model system: a *syn*-carbocupration TS in which the two C–O bonds are aligned was computed to be energetically preferred over isomeric Cu enolates and alternative mechanisms involving hydrogen-transfer to the terminal alkyne from an enol nucleophile (Figure S1). Models were also considered in which the Cu counterion (chloride) was still present in the carbocylization step; however, the computed activation free-energy barrier of C–C bond formation is around 10 kcal mol^{-1} higher than for a Cu/amine complex (see Figure S2 in the Supportig Information) and thus these other models were discounted. We thus focussed on the computational description of the carbocyclization step shown in Figure 9. In our model, a simplified structure lacking the olefin substituent on the quinuclidine was used to describe the pre-catalyst **1b**. This modelling assumption is justified by the similar *ee* (with opposite sign) obtained when using pseudoenantiomeric pre-catalyst **1d**, differing only in the positioning of the vinyl substituent. For substrate **2a** and model pre-catalyst **1b**, we performed a number of optimizations starting from different geometries of the pre-catalyst with respect to the cyclic core of the TS. This search process yielded eight unique conformations (four enolate *Re* face attack, four enolate *Si* face) from which the lowest-energy and thus most important diastereomeric pair, making up 87% of the conformer distribution at 298 K, are shown below in Figure 9.

The low-energy TSs are both characterized by a six-membered cyclic TS in which the alkyne and enolate are both coordinated to Cu^{I}. The *syn*-carbometallation across the alkyne of these models is consistent with the experimentally

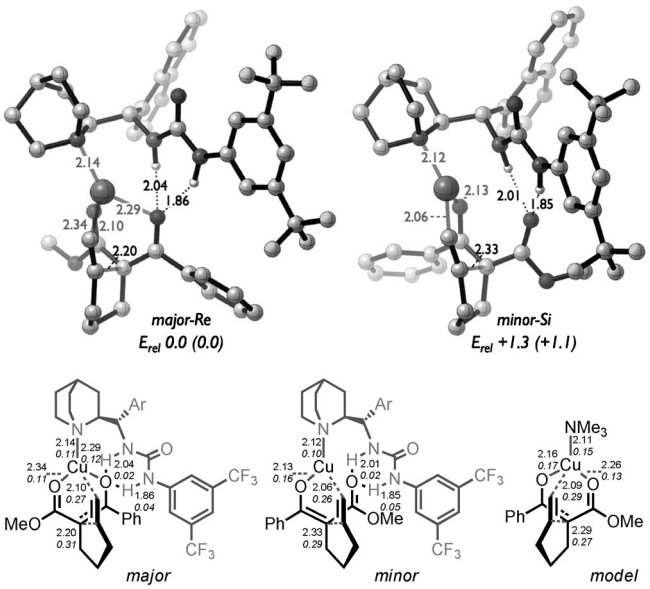

Figure 9. Top: Optimized M062X/6-31G(d) structures of lowest-energy competing TSs for C–C bond formation of **2a** catalyzed by a simplified version of **1b** (H atoms are omitted for clarity). ZPE-inclusive M062X/6-31G(d) relative energies, with M062X/6-311+G(d,p) in parentheses, shown in kcal mol^{-1}. Bottom: Wiberg bond orders and distances (Å) for key interactions in the TSs and for a simplified model.

observed stereoselectivity of deuterium incorporation in Scheme 1. Pre-catalyst coordination to Cu^{I} occurs through the quinuclidine nitrogen atom, leaving the urea group to hydrogen bond with one of the oxygen atoms. Coordination of the urea oxygen to Cu is disfavored by ca. 13 kcal mol^{-1}, and other H-bonding modes were calculated; however, the pre-catalyst scaffold evidently favours the mode shown in Figure 9. The optimized TS geometries for enolate *Re* and *Si* face attack show the former is favored by 1.3 kcal mol^{-1}, in accord with experiment in which this is the major enantiomer in 92% *ee* (the M062X/6-31G(d) computed *ee* from competing Boltzmann factors is 82%).

One marked structural difference between the diastereomeric TSs that could account for the facial selectivity is the lack of any ester O–Cu interaction in the disfavored TS. The metal plays a dual role in the Conia-ene TS: to coordinate strongly to the charged β-dicarbonyl enolate while also activating the η^2-coordinated alkyne. It is the former of these two roles that differs between the *Re* and *Si* TS. Relative to a trimethylamine: a Cu^{I} model system lacking any hydrogen-bonding contributions, the effect of the two H-bonding interactions formed between the urea group and one of the oxygen atoms is to weaken the strength of the corresponding O–Cu interaction. This is evident from bond distances and calculated bond orders (BOs) in Figure 9, in which relative to a model TS, the ketone O–Cu interaction lengthens by 0.13 Å and loses 0.05 in terms of BO in the major TS, and the ester O–Cu interaction effectively disappears in the minor TS. The strength of hydrogen-bonding interactions is very similar for the two TSs, as judged by O–H distances and computed BOs, and serves to compensate for the loss of

Cu–O bonding. However, critically in the major TS urea coordination occurs at the more electron-rich ketone oxygen, which is able to remain bound to Cu, whereas in the minor TS the ester oxygen atom is unable to do both and sacrifices Cu coordination to engage in hydrogen bonding. Further calculations on the model of pre-catalyst **1b** with a substrate possessing an aliphatic ketone (c.f. Table 4, methyl ketones **3o**, **3p**, and ethyl ketone **3q**) yield a computed selectivity of 93% in favour of *Re*-face attack, in accord with experiment (79–83% *ee*). Pre-catalyst **1t** gives comparable selectivity in experiment (81% *ee*) and the computed selectivity again is in good agreement, albeit slightly overestimated, at 95% *ee*. Competing transition structures are shown below in Figure 10. A common mode of stereoinduction is seen for

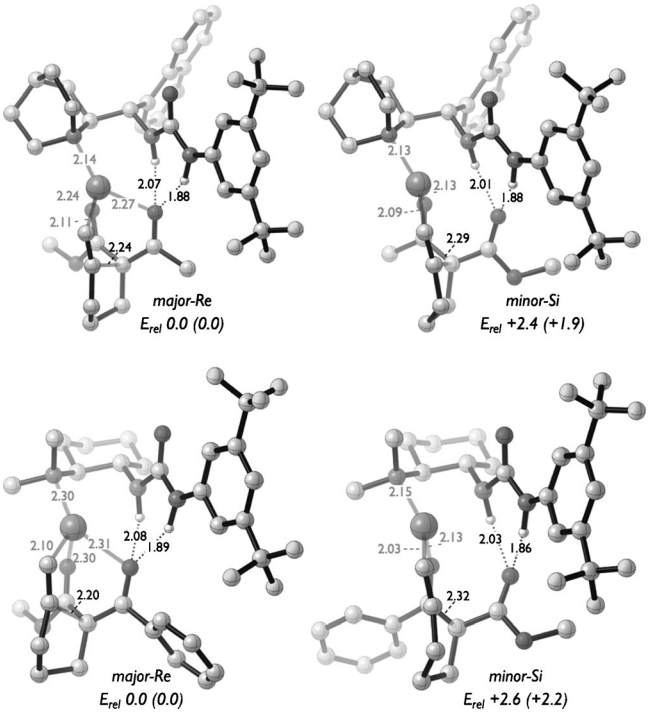

Figure 10. Optimized M062X/6-31G(d) structures of lowest-energy competing TSs for C–C bond formation (H atoms are omitted for clarity) of **3o** catalyzed by simplified **1b** (top) and of **3a** catalyzed by **1t** (bottom). ZPE-inclusive M062X/6-31G(d) relative energies, with M062X/6-311+G-(d,p) in parentheses, shown in kcal mol^{-1}, distances in (Å).

all of the substrates and pre-catalysts studied computationally: in enolate *Si*-face attack the ester carbonyl O–Cu interaction is lost at the expense of two hydrogen bonds to the urea of the pre-catalyst, whereas the major pathway preserves both of these stabilizing interactions.

Conclusion

On the basis of the experimental evidence and computational modeling described above, we propose the catalytic cycle shown in Scheme 3, in which the amino urea pre-catalyst **1b**

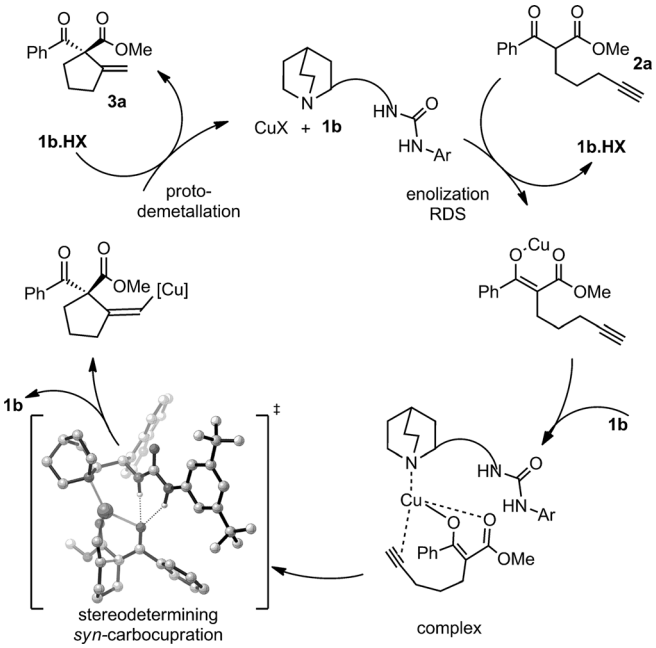

Scheme 3. Proposed catalytic cycle.

is involved in two distinct roles: ligating to the Cu^{I} and promoting enolization and subsequent formation of a reactive copper enolate that undergoes *syn*-carbocupration. The formation of a 1:1 [Cu]/[pre-catalyst] complex is supported by nonlinear studies (see Figure 8). Background enolization involving **1b** without Cu is possible, but ultimately unproductive. Cu is certainly present in the rate-limiting enolization step (since the order with respect to Cu is non-zero), which is then followed by *syn*-carbocupration, a cyclization mechanism supported by deuterium labeling and predicted by DFT studies to be the lowest energy pathway. Ligation of **1b** to the Cu-enolate imparts asymmetry in the stereodetermining C–C bond-forming step. Computed relative energetics for the diasteromeric transition structures are in good agreement with observed levels of enantioselectivity. Final protodemetallation furnishes the cyclized product **8** and regenerates pre-catalyst **1b**. The urea group of the pre-catalyst plays a key role through hydrogen-bonding interactions with the oxygen atom of the enolized ketone, which provides additional organization to discriminate the diastereomeric transition structures.

Experimental Section

General procedure for Conia-ene cyclizations: The β-ketoester or β-ketoamide **2a–r** (0.2 mmol) was added to a solution of CuOTf·$^{1}/_{2}$C$_6$H$_6$ (2.5 mg, 0.01 mmol) and **1a–t** (22 mg, 0.04 mmol) in dry CH_2Cl_2 (2 mL). The mixture was stirred at room temperature until complete consumption of the β-ketoester or β-ketoamide was indicated by TLC analysis. The solvent was then removed under reduced pressure and the crude product obtained was purified by flash column chromatography.

Acknowledgements

We thank the EPSRC (Leadership Fellowship to D.J.D., postdoctoral fellowships to F.S.), the Oxford University Press John Fell fund (R.S.P.) the European Community (IEF to F.S. (PIEF-GA-2009-254068)), the Spanish Ministerio de Educación (MEC) for a FPU and a summer stay fellowship to A.L.F.A. We are grateful to T. Claridge and B. Odell of the Department of Chemistry, University of Oxford, for essential and precious assistance with the use of NMR spectroscopy for kinetic measurements and data interpretation. We acknowledge the use of the EPSRC UK National Service for Computational Chemistry Software (NSCCS) at Imperial College London and contributions from its staff in carrying out this work.

[1] a) A. G. Doyle, E. N. Jacobsen, *Chem. Rev.* **2007**, *107*, 5713–5743; b) M. Shibasaki, M. Kanai, S. Matsunaga, N. Kumagai, *Acc. Chem. Res.* **2009**, *42*, 1117–1127; c) S. Matsunaga, M. Shibasaki, *Bull. Chem. Soc., Jpn.* **2008**, *81*, 60–75; d) R. M. Haak, S. J. Wezenberg, A. W. Kleij, *Chem. Commun.* **2010**, *46*, 2713–2723; e) S. J. Connon, *Chem. Commun.* **2008**, 2499–2510; f) E. N. Jacobsen, *Acc. Chem. Res.* **2000**, *33*, 421–431; g) S. Saito, H. Yamamoto, *Acc. Chem. Res.* **2004**, *37*, 570–579; h) A. Lattanzi, *Chem. Commun.* **2009**, 1452–1463; i) F. Giacalone, M. Gruttadauria, P. Agrigento, R. Noto, *Chem. Soc. Rev.* **2012**, *41*, 2406–2447; j) A. E. Allen, D. W. C. MacMillan, *Chem. Sci.* **2012**, *3*, 633–658.

[2] a) L. Stegbauer, F. Sladojevich, D. J. Dixon, *Chem. Sci.* **2012**, *3*, 942–958; b) P. de Armas, D. Tejedor, F. García-Tellado, *Angew. Chem.* **2010**, *122*, 1029–1032; *Angew. Chem. Int. Ed.* **2010**, *49*, 1013–1016; c) J. R. Gareth, *Tetrahedron* **2001**, *57*, 1865–1882; d) Y. J. Park, J.-W. Park, C.-H. Jun, *Acc. Chem. Res.* **2008**, *41*, 222–234; e) M. Rueping, R. M. Koenigs, I. Atodiresei, *Chem. Eur. J.* **2010**, *16*, 9350–9365; f) C. Zhong, X. Shi, *Eur. J. Org. Chem.* **2010**, 2999–3025; g) D. T. Cohen, K. A. Scheidt, *Chem. Sci.* **2012**, *3*, 53–57; h) C. Grondal, M. Jeanty, D. Enders, *Nat. Chem.* **2010**, *2*, 167–178; i) C. C. J. Loh, D. Enders, *Chem. Eur. J.* **2012**, *18*, 10212–10225; j) Z. Du, Z. Shao, *Chem. Soc. Rev.* **2013**, *42*, 1337–1378; k) W. Tang, S. Johnston, J. A. Iggo, N. G. Berry, M. Phelan, L. Lian, J. Bacsa, J. Xiao, *Angew. Chem.* **2013**, *125*, 1712–1716; *Angew. Chem. Int. Ed.* **2013**, *52*, 1668–1672.

[3] J. Ye, D. J. Dixon, P. S. Hynes, *Chem. Commun.* **2005**, 4481–4483.

[4] a) T. Yang, A. Ferrali, F. Sladojevich, L. Campbell, D. J. Dixon, *J. Am. Chem. Soc.* **2009**, *131*, 9140–9141; b) B. K. Corkey, F. D. Toste, *J. Am. Chem. Soc.* **2005**, *127*, 17168–17169; c) A. Matsuzawa, T. Mashiko, N. Kumagai, M. Shibasaki, *Angew. Chem.* **2011**, *123*, 7758–7761; *Angew. Chem. Int. Ed.* **2011**, *50*, 7616–7619.

[5] For selected racemic examples of cyclization of active methylene compounds into unactivated alkynes, see: a) J. M. Conia, P. Le Perchec, *Synthesis* **1975**, 1–19; b) J. J. Kennedy-Smith, S. T. Staben, F. D. Toste, *J. Am. Chem. Soc.* **2004**, *126*, 4526–4527; c) Q. Gao, B.-F. Zheng, J.-H. Li, D. Yang, *Org. Lett.* **2005**, *7*, 2185–2188; d) D. Bouyssi, N. Monteiro, G. Balme, *Tetrahedron Lett.* **1999**, *40*, 1297–1300; e) W. Hess, J. Burton, *Adv. Synth. Catal.* **2011**, *353*, 2966–2970; f) Y. Liu, R.-J. Song, J.-H. Li, *Synthesis* **2010**, *21*, 3663–3669; g) S. Montel, D. Bouyssi, G. Balme, *Adv. Synth. Catal.* **2010**, *352*, 2315–2320; h) C.-L. Deng, R.-J. Song, Y.-L. Liu, J.-H. Li, *Adv. Synth. Catal.* **2009**, *351*, 3096–3100; i) W. Li, X.-Z. Liu, X.-F. Zhou, C.-S. Lee, *Org. Lett.* **2010**, *12*, 548–551; j) S. Hatakeyama, *Pure Appl. Chem.* **2009**, *81*, 217–226; k) Y. Itoh, H. Tsuji, K.-I. Yamagata, K. Endo, I. Tanaka, M. Nakamura, E. Nakamura, *J. Am. Chem. Soc.* **2008**, *130*, 17161–17167; l) C.-L. Deng, T. Zou, Z.-Q. Wang, R.-J. Song, J.-H. Li, *J. Org. Chem.* **2009**, *74*, 412–414; m) K. Takahashi, M. Midori, K. Kawano, J. Ishihara, S. Hatakeyama, *Angew. Chem.* **2008**, *120*, 6340–6342; *Angew. Chem. Int. Ed.* **2008**, *47*, 6244–6246; n) C.-L. Deng, R.-J. Song, S.-M. Guo, Z.-Q. Wang, J.-H. Li, *Org. Lett.* **2007**, *9*, 5111–5114; o) J.-H. Pan, M. Yang, Q. Gao, N.-Y. Zhu, D. Yang, *Synthesis* **2007**, *16*, 2539–2544; p) J. S. Fisk, J. J. Tepe, *J. Am. Chem. Soc.* **2007**, *129*, 3058–3059; q) G. Eglinton, M. C. Whiting, *J. Chem. Soc.* **1953**, 3052–3059.

[6] See the Supporting Information for details.

[7] For selected examples of the DMSO effect in transition-metal catalysis, see: a) K. K. Spektor, G. L. Starova, Y. M. Skripkin, L. V. Stepakova, *Russ. J. Gen. Chem.* **2011**, *81*, 1772–1777; <lit b> M. S. Chen, M. C. White, *J. Am. Chem. Soc.* **2004**, *126*, 1346–1347.

[8] For example, DMSO titration experiments are used to estimate the strength of hydrogen-bonding in solution: a) T. P. Pitner, D. W. Urry, *J. Am. Chem. Soc.* **1972**, *94*, 1399–1400; b) M. Iqbal, P. Balaram, *J. Am. Chem. Soc.* **1981**, *103*, 5548–5552; c) P. A. Raj, P. Balaram, *Biopolymers* **1985**, *24*, 1131–1146.

[9] The reaction was quenched and analyzed after 3 h (25% conversion, *E*/*Z* 94:6) to minimize the extent of Cu^{I}-promoted H/D exchange processes in **4** prior to cyclization.

[10] a) D. A. Singleton, A. A. Thomas, *J. Am. Chem. Soc.* **1995**, *117*, 9357–9358; b) K.-H. Kwon, D. W. Lee, C. S. Yi, *Organometallics* **2010**, *29*, 5748–5750; c) Y. Wu, R. P. Singh, L. Deng, *J. Am. Chem. Soc.* **2011**, *133*, 12458–12461.

[11] Reported BEMP PK_{bH+}(MeCN) is 27.6 according to: R. Schwesinger, H. Schlemper, *Angew. Chem.* **1987**, *99*, 1212; *Angew. Chem. Int. Ed. Engl.* **1987**, *26*, 1167 and quinuclidine $PK_{bH+}(H_2O)$ is 11.4 according to: E. A. Castro, M. Aliaga, P. Campodónico, J. G. Santos, *J. Org. Chem.* **2002**, *67*, 8911; no PK_{bH+} measurement for the two compounds in the same solvent were found by the authors. As a comparison the PK_{bH+}(MeCN) values for some representative nitrogen bases are as following: NEt_3 (18.82), *N*-methyl-piperidine (18.25), sparteine (21.66), DBU (24.34), TMG (23.3). All values according to: E. I. Rõõm, A. Kütt, I. Kaljurand, I. Koppel, I. Leito, I. A. Koppel, M. Mishima, K. Goto, Y. Miyahara, *Chem. Eur. J.* **2007**, *13*, 7631–7643.

[12] V. Chandrasekhar, P. Thilagar, B. Murugesa Pandian, *Coord. Chem. Rev.* **2007**, *251*, 1045–1074.

[13] C. Girard, H. B. Kagan, *Angew. Chem.* **1998**, *110*, 3088–3127; *Angew. Chem. Int. Ed.* **1998**, *37*, 2922–2959.

[14] a) T. Okino, Y. Hoashi, T. Furukawa, X. Xu, Y. Takemoto, *J. Am. Chem. Soc.* **2005**, *127*, 119–125; b) A. Berkessel, F. Cleemann, S. Mukherjee, T. N. Mueller, J. Lex, *Angew. Chem.* **2005**, *117*, 817–821; *Angew. Chem. Int. Ed.* **2005**, *44*, 807–811.

[15] a) N. Iwasawa, Y. Hayashi, H. Sakurai, K. Narasaka, *Chem. Lett.* **1989**, *18*, 1581–1584; b) C. Bolm, G. Schlingloff, K. Harms, *Chem. Ber.* **1992**, *125*, 1191–1203.

[16] Gaussian 09, Revision A.02, M. J. Frisch et al., Gaussian, Inc. Wallingford, CT, **2009**.

[17] Y. Zhao, D. G. Truhlar, *Theor. Chem. Acc.* **2008**, *120*, 215–241.

[18] a) A. D. Becke, *J. Chem. Phys.* **1993**, *98*, 5648–5652; b) C. Lee, W. Yang, R. G. Parr, *Phys. Rev. B* **1988**, *37*, 785–789; c) S. H. Vosko, L. Wilk, M. Nusair, *Can. J. Phys.* **1980**, *58*, 1200–1211; d) P. J. Stephens, F. J. Deulin, C. F. Chabalowski, N. J. Frisch, *J. Phys. Chem.* **1994**, *98*, 11623–11627.

[19] R. S. Paton, J. M. Goodman, *J. Chem. Inf. Model.* **2009**, *49*, 944–955.

[20] R. R. Knowles, E. N. Jacobsen, *Proc. Natl. Acad. Sci. USA* **2010**, *107*, 20678–20685.

[21] a) G. O. Jones, P. Liu, K. N. Houk, S. L. Buchwald, *J. Am. Chem. Soc.* **2010**, *132*, 6205–6213; b) H.-Z. Yu, Y.-Y. Jiang, Y. Fu, L. Liu, *J. Am. Chem. Soc.* **2010**, *132*, 18078–18091.

[22] P. J. Hay, W. R. Wadt, *J. Chem. Phys.* **1985**, *82*, 299–310.

[23] a) D. Feller, *J. Comput. Chem.* **1996**, *17*, 1571–1586; b) K. L. Schuchardt, B. T. Didier, T. Elsethagen, L. Sun, V. Gurumoorthi, J. Chase, J. Li, T. L. Windus, *J. Chem. Inf. Model.* **2007**, *47*, 1045–1052.

[24] S. E. Wheeler, K. N. Houk, *J. Chem. Theory Comput.* **2010**, *6*, 395–404.

[25] Y. Takano, K. N. Houk, *J. Chem. Theory. Comput.* **2005**, *1*, 70–77.

[26] E. D. Glendening, A. E. Reed, J. E. Carpenter, F. Weinhold, NBO Version 3.1.

[27] K. A. Wiberg, *Tetrahedron* **1968**, *24*, 1083–1096.

Received: March 12, 2012
Revised: June 29, 2013
Published online: ■■ ■■, 0000

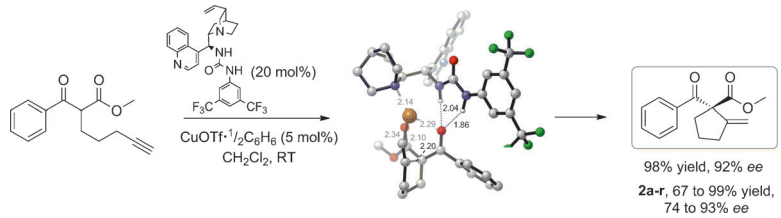

Cooperation is key! A detailed mechanistic study on the enantioselective Conia-ene reaction catalyzed by cinchona-derived amino urea pre-catalysts and Cu^{I} is reported (see scheme; Tf = trifluoromethanesulfonate). A combination of experimental considerations and quantum mechanical calculations has been carried out to prove the cooperative nature of the system and propose a plausible catalytic cycle.

Reaction Mechanism

F. Sladojevich, Á. L. Fuentes de Arriba, I. Ortín, T. Yang, A. Ferrali, R. S. Paton, D. J. Dixon* . .* ▮▮▮▮–▮▮▮▮

Mechanistic Investigations into the Enantioselective Conia-Ene Reaction Catalyzed by Cinchona-Derived Amino Urea Pre-Catalysts and Cu^{I}